ELSEVIER

Journal of Alloys and Compounds 446–447 (2007) 534–538

Journal of ALLOYS AND COMPOUNDS

www.elsevier.com/locate/jallcom

Studies on hydrogen loaded V–Fe8 at% films on Al_2O_3 substrate

R. Gemma, T. Al-Kassab, R. Kirchheim, A. Pundt *

Institute of Material Physics, University of Göttingen, Friedrich-Hund-Platz 1, D-37077 Göttingen, Germany

Received 1 November 2006; received in revised form 16 January 2007; accepted 18 January 2007
Available online 23 January 2007

Abstract

Hydride formation of V–Fe8 at% films with different microstructures was investigated by measuring the electromotoric force (EMF), in-plane stress and, additionally, the local chemistry by performing tomographic atom probe (TAP). The phase boundaries of the films were found to be microstructure dependent: the α-phase solubility limit was found to be $c_{H,\alpha} = 0.1$ H/V and $c_{H,\beta} = 0.45 \pm 0.02$ H/V for films with small-domain size, and $c_{H,\alpha} = 0.1$ H/V and $c_{H,\beta} = 0.6 \pm 0.02$ H/V for films with large domain size. Stress release also depends on the microstructure; it is more efficient for small-domain samples resulting in smaller total stress. It is shown that the plateau pressure and the plateau slope of the films increase with hydrogen-induced in-plane compressive stress increase. TAP analysis at about 20 K monitors the occurrence of a plate-like hydride $VD_{0.65}$-precipitate at the V/Pd interface. The detected concentrations are in good agreement with those expected at low temperatures.

Keywords: Hydrogen absorbing materials; Thin films; Electromotive force; Elasticity

1. Introduction

It is well known that hydriding properties of metallic thin films differ from those of bulk because of different microstructure and because the metal film is clamped to a substrate and, has in-plane stress. Stress and corresponding strain can change thermodynamics of the M–H reaction [1–4]. Interesting results have been reported on Fe/V mutilayers, showing changes in the solubility at the interfaces of adjacent layers [3]. These changes are attributed to the electronic charge transfer. However, Kesten et al. [5] reported on a certain solubility of Fe in V layers also changing the overall hydrogen solubility. The estimated Fe concentration was 8 at%. The Fe was homogeneously distributed, which is in a good accordance with the concentration being in the α-phase of the Fe–V phase diagram [6].

To address the properties of the V–8 at%Fe layers on the hydrogen uptake themselves, we investigate in this study the phase boundaries of ternary H–V–8 at%Fe films with different microstructures by electromotive force (EMF) measurement and simultaneous stress measurement. With use of this combination, one can investigate the thermodynamics as well as the stress response of the film during hydrogen absorption at moderate temperatures. Additionally, tomographic atom probe (TAP) analysis and field ion microscope (FIM) imaging of deuterium-loaded films was carried out in order to investigate its local microstructure and deuteride formation. The TAP measures single atoms by time-of-flight and, therefore, hydrogen atoms can be detected together with metal atoms. Accordingly, the three-dimensional structure of the measured sample can be obtained on atomic scale. Generally the depth resolution of this analysis is in sub-Angstrom, which is suitable especially for studying multilayer's interfaces.

2. Experimental

V–8 at%Fe film samples with 100 nm thickness were prepared on 0.2 mm thick Al_2O_3(0 0 0 1) substrates (7 mm × 30 mm) by ion beam sputter deposition under Ar atmosphere at the pressure of 5×10^{-3} Pa, with the deposition rate of 0.4 nm/min. The substrate temperature during deposition was selected as 297, 573, 773 and 1073 K. At those temperatures, the base pressure of the sputter chamber ranged from 1×10^{-8} to 2×10^{-6} Pa, respectively. After cooling down to room temperature the V–8 at%Fe surface was capped with 20 nm Pd layer to prevent the film from oxidation and to facilitate hydrogen dissociation. The out-of-plane and in-plane crystal structures of the films were subsequently studied by XRD (Philips, X'pert) rocking scans and texture measurements. Stress evolution in the film samples during hydrogen loading was measured by using the house-made bending setup. Details about this setup were published elsewhere [7]. With the help of this system it is possible to measure EMF curve and stress curve as a function of the hydrogen concentration simultaneously.

* Corresponding author. Tel.: +49 551 39 5007; fax: +49 551 39 5012.
E-mail address: apundt@ump.gwdg.de (A. Pundt).

0925-8388/$ – see front matter © 2007 Elsevier B.V. All rights reserved.
doi:10.1016/j.jallcom.2007.01.099

The hydrogen loading was carried out electrochemically by using a mixed solution of phosphoric acid and glycerin (1:2 in volume) as the electrolyte. A Ag/AgCl(sat.) and Pt wires were used as the reference and the counter electrode, respectively. Before each measurement the residual hydrogen in the sample was removed by applying positive voltage of about 0.4 V for several minutes. All results were obtained during the first loading of the samples.

V–Fe8 at% films were also prepared at 297 K for tomographic atom probe (TAP) analysis [8] and FIM with the thickness of 5–10 nm followed by Pd capping. They were deposited in the same way as described above but on needle-shaped W substrates with a tip curvature radius of ~50 nm. These V tips were loaded with D_2 gas in an external chamber at 295 K and 200 Pa for 12 h before analyzing with TAP. Deuterium was used in order to suppress the diffusion at 20 K because hydrogen was found to be mobile even at 20 K [5].

This TAP analysis has a strong advantage for atomic scale investigation. The principle can be simply described as follows [8]: by applying timing pulse voltage to the tip, surface atoms are removed by field evaporation and after several nanoseconds, collected at a two-dimensional position sensitive detector. For each atom the time-of-flight and the impact of the position is measured and, therefore, the elemental species and its position can be successfully identified by taking the simple projection geometry [9] into account.

The obtained data are finally reconstructed into three-dimension. As a sequence, it becomes possible to look into the sample on atomic scale.

3. Results and discussion

Fe concentration in V was checked by EDX and found to be 8 ± 1 at% for all of the samples.

In Fig. 1, the results of θ–2θ XRD scans of the samples are shown together with their rocking scans in the inset. The reference 2θ position of bulky V–8 ± 1 at%Fe alloy was obtained by using experimental data of [10]. The obtained parameters for V–8 ± 1 at%Fe alloy are $d_{(1\,1\,0)} = 0.2124(2)$ nm and $a = 0.3003(2)$ nm. Each film shows preferential growth in [1 1 0]-direction regardless of substrate temperature. However, the peak position shifts towards higher 2θ angle with the temperature, which implies that a higher deposition temperature is correlated to a larger out-of-plane compression. This trend can be explained by considering the difference in thermal expansion coefficients α_{th} of V and Al_2O_3. During cooling down, the difference in α_{th} makes the film to shrink more than the substrate does. Since shrinking is not possible when the film is clamped to the substrate, this leads to in-plane tensile stress between film and substrate. This tensile stress increases with increasing temperature difference. Because of converse-contraction, in-plane tensile stress is accompanied by out-of-plane lattice contraction showing the described temperature dependence. The obtained (1 1 0) lattice plane distance and corresponding degree of expansion (+) and compression (−) in out-of-plane (1 1 0) lattice plane distance calculated by using reference data of d(1 1 0) are shown in Table 1.

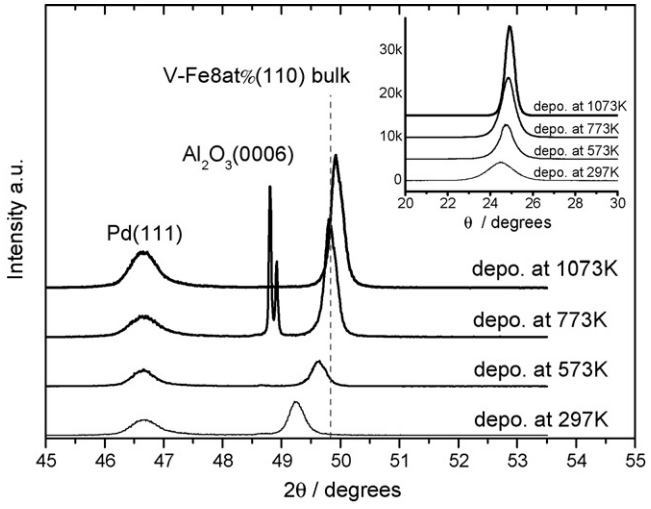

Fig. 1. $2\theta/\theta$ XRD profiles of V–Fe8 at% films deposited at 297, 573, 773 and 1073 K. The 2θ position of V–Fe8 at% bulk taken from Ref. [9] is also shown together. Inset shows the rocking curve of each sample.

Table 1
The out-of-plane lattice distance d(1 1 0) and lattice parameter a of V–Fe8 at% film

	d(1 1 0) (nm)	a (nm)	$d - d_{ref.}/d_{ref.}$ (%)
Ref. V–Fe8 at% alloy	0.2124(2)	0.3003(2)	–
297 K	0.2147	0.3037	1.13
573 K	0.2133	0.3017	0.46
773 K	0.2125	0.3005	0.05
1073 K	0.2119	0.3000	−0.23

Reference data of V–Fe8 at% bulk [9] are also shown.

The rocking curves show a FWHM of the peak decreasing from 1.7° to 0.4° with increasing temperature. Thus, the domain size strongly increases with increasing temperature. According to the results of texture measurement, all of the films were found to have V–Fe8 at%(1 1 0)//Al_2O_3(0 0 0 1) orientation with preferential in-plane adjustment of the lattices, meaning epitaxial growth. The pole figure of the V–Fe8 at%(1 1 0) deposited at 297 K is shown in Fig. 2a, as an example. Black, or gray shaded regions indicate peaks visible by height contours. Considering the three-fold symmetry of the substrate, at least three domains (marked with I, II, and III) are visible in V–Fe8 at% layer, in approximately 60° in-plane rotation. Slight distortions can be seen. Such a multiple domain formation was also observed in Fe/GaN system [11]. The picture of Al_2O_3(0 0 0 1) was adopted from [12]. The lattice mismatch was expected to be 10% in case of the configuration shown in Fig. 2b. Even with such a huge misfit epitaxial growth of thick films can happen, when misfit dislocations are implemented. Since our films have thickness of 100 nm, it is, therefore, reasonable to note that our films contain semi-coherent interface where many misfit dislocations are present. Since the pole-figures of all films were similar, the interpretation is also true for the other films.

The results of EMF measurements during hydrogen loading of the three different films, carried out at 294 K, are shown in Fig. 3. Before each measurement the sample was shortly discharged using constant voltage to remove residual hydrogen. All the results shown below are those of the first loading. An ideal curve according to Sieverts' law is also plotted. At concentrations close to 10^{-1} H/V, Sieverts' law holds. Considerable deviation to downwards from the ideal curve can be interpreted as the H trapping at dislocations, which is more obvious for the film deposited at 1073 K.

The plateau pressure of all three samples is elevated compared to that of V–H thin films. This plateau pressure was derived by using data from Andersson et al. [13], who reported P–C–T curves of 50 and 100 nm epitaxial vanadium films, taken at

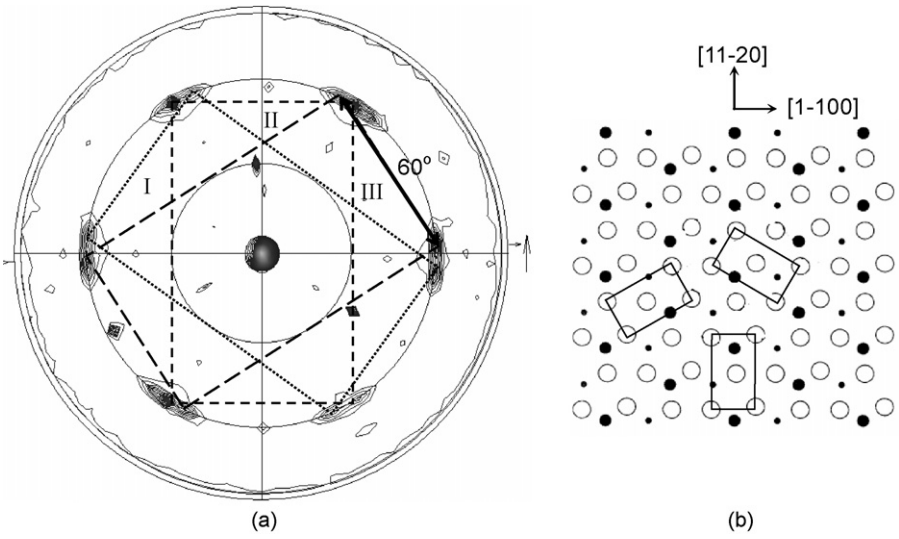

Fig. 2. (a) Pole figure of V–Fe8 at%(1 1 0). The sample was deposited at 297 K. (b) Al_2O_3(0 0 0 1) surface and possible in-plane configuration of V atoms. White circle: O atom, small black circle: bottom Al atom and large black circle: upper Al atom (Al_2O_3(0 0 0 1) plane configuration was adopted from [12]).

high temperatures. According to an extrapolation of the van't Hoff's plots of those films to 294 K, the expected plateau pressure of vanadium will be 10^{-3} Pa. This value is considerably smaller than that of the samples measured here. An increase of the plateau pressure can be explained by the alloying effect. As has already been published by Yukawa et al. [14], who studied the stability of vanadium hydride (V_2H and VH_2) alloyed with various transition metals, a drastic increase of the chemical potential was reported for V_2H when several mol% Fe were alloyed. Regarding their results on V–Fe alloy with concentrations up to 6%, one can graphically obtain the following relationship between Fe concentration, c_{Fe} (at%) and plateau pressure of $VH_{0.25}$, $p_{VH_{0.25}}$, assuming linear relationship of the plot in Fig. 4a in [14]:

$$\ln\frac{p}{p_0} = 0.7675 c_{Fe} \quad (1)$$

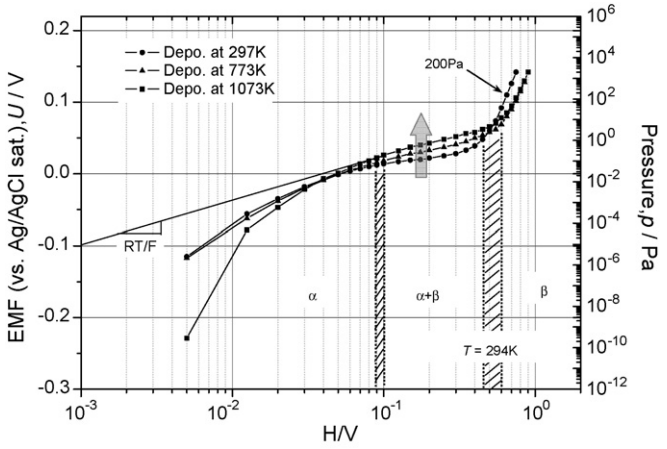

Fig. 3. EMF curves of V–Fe8 at% films deposited at 297, 773 and 1073 K. Shaded regions correspond to phase boundaries that depend on the samples. The plateau pressure as well as its slope increases with the deposition temperature. The arrow pointing at 200 Pa indicates the $H_2(D_2)$ pressure applied for the samples for TAP analysis, at which β hydride is expected to form.

where p and p_0 are the plateau pressure of the alloyed sample and pure vanadium, respectively. If we can extend that the relation in Eq. (1) to 8 at%Fe and also, the van't Hoff's plot of Andersson et al. to 294 K, we can expect the dissociation pressure $p_{0.25} = 0.6 \pm 0.3$ Pa at 294 K. The experimental data are in good accordance to this pressure.

However, it also should be noticed that the plateau pressure increases with increasing the deposition temperature. This increase will be addressed in the following. The different microstructure of the film (see Fig. 1, rocking curves), is not likely to change the plateau pressure [15].[1] But, since out-of-plane compressive strain was detected in the samples, one should think about the stress contribution on the hydride stability.

In Fig. 4, we have plotted the results of stress measurements, simultaneously carried out with the EMF measurement, i.e. hydrogen loading of Fig. 3. In the α-phase region (for low concentrations below H/V = 0.1), the linear increase of compressive stress with a slope of −11.9 GPa/c_H was confirmed. Since the films are clamped to elastically hard substrates, the elastic volume expansion due to hydrogen absorption can take place only in out-of-plane direction z at low H concentrations. According to linear elasticity theory of bcc materials, the expected compressive stress in ⟨1 −1 0⟩-direction, and ⟨0 0 1⟩-direction are calculated by using the following equations [16]:

$$\sigma[1\ -1\ 0] = -4\left(\frac{(C_{11}+2C_{12})C_{44}}{C_{11}+C_{12}+2C_{44}}\right)\varepsilon_0' \quad (2)$$

$$\sigma[0\ 0\ 1] = -\left(\frac{2(C_{11}+2C_{12})C_{44}+C_{11}^2+C_{11}C_{12}-2C_{12}^2}{C_{11}+C_{12}+2C_{44}}\right) \times \varepsilon_0' \quad (3)$$

[1] But solubility limits can be affected, since the domain boundaries are not likely to participate in hydride formation.

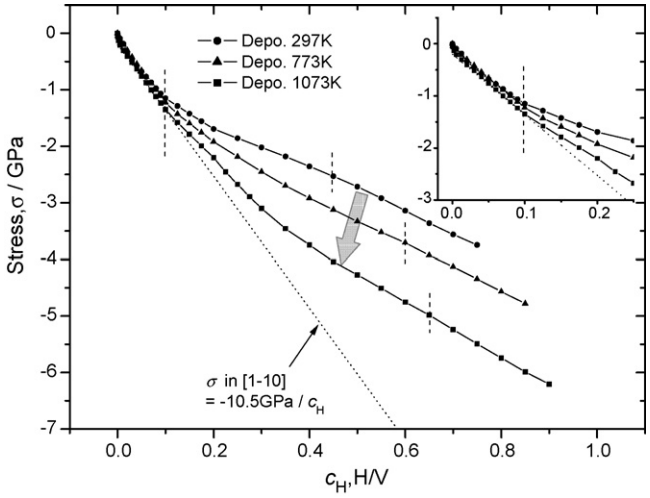

Fig. 4. Stress curves of V–Fe8 at% films deposited at 297, 773 and 1073 K during hydrogen absorption simultaneously obtained with EMF measurement. The stress release is efficient in case of the samples deposited at lower temperatures.

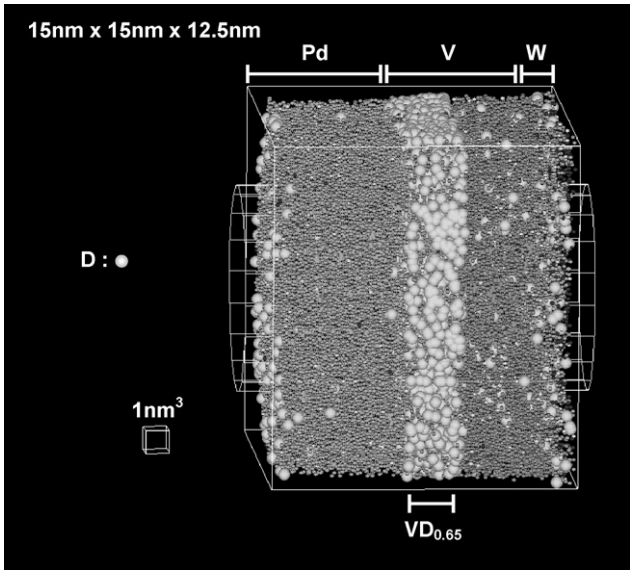

Fig. 5. Three-dimensional reconstruction of TAP data for V–Fe8 at% film deposited on W(1 1 0) tip and subsequently loaded with 200 Pa D_2 gas at room temperature. A big white sphere shows D atom. During the field evaporation the temperature was kept at $T = 22$ K.

Here, the $C_{11} = 229$ GPa, $C_{12} = 119$ GPa, and $C_{44} = 43$ GPa according to the reference for vanadium bulk [17]. The last parameter ε_0' is an expansion coefficient of the material by hydrogen absorption, given by α_H/c_H. Taking $c_H = 1$, one can obtain $\varepsilon_0' = 0.063$ by using $\alpha_H = 0.063$ [18] for single crystal vanadium. By taking the average of the products in Eqs. (2) and (3), one can get $\sigma' = -10.5$ GPa. This value is consistent with the observed slope of the plot shown in Fig. 4, even though we used the elastic constants of bulk V. This hints on a uniaxial expansion in the α-phase region. Those of V–Fe alloy are unpublished. In the inset of Fig. 4 the magnified part of the plot is shown so that one can see the deviation from the linear behavior of the stress evolution. At this inflection point the phase transition starts and the hydrogen-induced stress decreases. This inflection seems to take place almost at the same concentration of $c_H = 0.1$ H/V for all of the films. This implies that the elastic responses of the films are nearly the same and, surprisingly, do not depend on the initial stress of the films.

In α + β region ($c_H = 0.1$–0.45 or 0.6 H/V) for different samples, the stress increase is larger for the films deposited at higher temperatures. When the concentration exceeds α + β region the slope of the stress curve changes again, as shown with dot lines across the curves. This trend is most pronounced in case of the film deposited at 297 K. Also, the stress release is most effective for this film. The total hydrogen related stress is −3.7 GPa for the film deposited at 297 K, and it is −5.5 GPa for the film deposited at 1073 K. Stress release, therefore, is more efficient for the film with smaller domains. This might hint on stress releasing processes like grain boundary sliding. Further investigations have to be performed to clarify this interpretation. To summarize, the stronger the compressive stress increase in the film, the steeper is the slope in the according two-phase region. This finding is marked with arrows in Figs. 3 and 4. The phase boundaries determined by EMF measurement and those obtained by stress measurement are in sufficient agreement.

In Fig. 5, the three-dimensional reconstruction of a TAP analysis is shown. Big white circles indicate deuterium atoms. The direction of analysis corresponds to ⟨1 1 0⟩. In FIM images (not shown here due to page limit) we have confirmed that V–8 at%Fe⟨1 1 0⟩ is parallel to W⟨1 1 0⟩, by checking the relative pole positions to be identical. This indicates that the top grain of the V–Fe8 at% layer was epitaxially grown with (1 1 0)-orientation on W(1 1 0). This epitaxially matched grain has a lateral diameter of more than 75 nm and is, therefore, much larger than the measured cube taken in the grain center with a lateral dimension of about 15 nm. At this distance, influences of grain boundaries on the obtained results are unlikely.

In Fig. 5 D atoms are found at Pd/V–8 at%Fe interface with extremely high density. At this region, the average D concentration was found to be $c_D = 0.65(7)$ D/V according to the concentration profile of shown in Fig. 6, indicates β-deuteride. It is close to the expected value because the concentration at 200 Pa gives $c_H = 0.64$ H/V (see plot 297 K in Fig. 3).[2] The thickness of the β-deuteride can be estimated as about 2 nm with lateral extension of more than 15 nm, hinting on a plate-like deuteride. The rest of the V–8 at%Fe film contains less than 0.10 D/V and, therefore is in the α-phase. It is surprising that we have D atoms distributed in a layer structure at the Pd–V interface. This kind of layer structure of the hydride was also found in Mg_2Ni films [20]. However, for epitaxial Nb-films and Gd-films, hydrides predominately form cylinders going right through the complete film [21,22]. The concrete explanation of the different morphology of the hydrides is not yet clear.

[2] The change of the dissociation pressure between the V–8 at%Fe–$H_{0.64}$ and the V–8 at%Fe–$D_{0.64}$ is assumed to be small, as in the case of V–D and V–H [19].

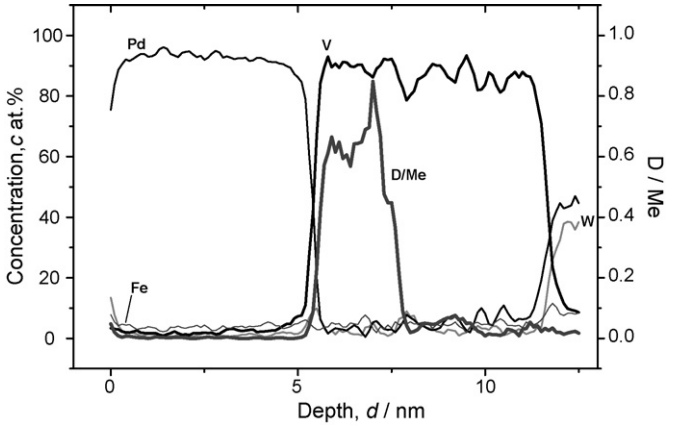

Fig. 6. Concentration profile of the reconstructed volume shown as the cylinder region in Fig. 5. The obtained D concentration near Pd/V interface was, $c_D = 0.65(7)$ D/V, indicating β hydride was formed here.

4. Conclusion

In this paper, the hydride formation of V–Fe8 at% films with different microstructures was investigated by EMF measurements combined with stress measurements and TAP. The phase boundaries of the films were found to be microstructure dependent. The α-solubility limit was found to be $c_{H,\alpha} = 0.1$ H/V and $c_{H,\beta} = 0.45 \pm 0.02$ H/V for films with small-domain size, and $c_{H,\alpha} = 0.1$ H/V and $c_{H,\beta} = 0.60 \pm 0.02$ H/V for films with large domain size. The plateau pressure and the plateau slope of V–Fe8 at% films increases with hydrogen-induced in-plane compressive stress increase. Stress release also depends on the microstructure; it is more efficient for small-domain samples. TAP analysis at about 20 K monitors the occurrence of a plate-like $VD_{0.65}$-precipitate at the Pd/V interface. The detected concentrations are in good agreement with those expected at low temperatures.

References

[1] H.A. Wriedt, R.A. Oriani, Acta Metall. 18 (1970) 753.
[2] P.R. Miceli, H. Zabel, J.E. Cunningham, Phys. Rev. Lett. 54 (1985) 917.
[3] B. Hjörvarsson, G. Andersson, E. Karlsson, J. Alloys Compd. 253–254 (1997) 51.
[4] A. Pundt, Adv. Eng. Mater. 6 (2004) 11.
[5] P. Kesten, A. Pundt, G. Schmitz, R. Kirchheim, J. Alloys Compd. 330–332 (2002) 225.
[6] T.B. Massalski, Binary Alloy Phase Diagrams, ASM International, Materials Park, OH, 1991.
[7] A. Pundt, E. Nikitin, P. Pekarski, R. Kirchheim, Acta Mater. 52 (2004) 1579.
[8] A. Bostel, D. Blavette, A. Menand, J.M. Sarrau, J. Phys. (Paris) Colloq. 50 (1989) C8-501.
[9] T. Al-Kassab, H. Wollenberger, G. Schmitz, R. Kirchheim, Tomography by atom probe field ion microscopy, in: M. Rühle, F. Ernst (Eds.), High Resolution and Spectrometry of Materials, Springer-Verlag, 2002.
[10] M. Shiga, Y. Nakamura, J. Phys. F: Met. Phys. 8 (1978) 177.
[11] R. Calarco, R. Meijers, N. Kaluza, V.A. Guzenko, N. Thillosen, Th. Schäpers, H. Lüth, M. Fonin, S. Krzyk, R. Ghadimi, B. Beschoten, G. Güntherodt, Phys. Status Solidi (a) 202 (2005) 754.
[12] J. Guo, D.E. Ellis, D.J. Lam, Phys. Rev. B 45 (1992) 13647.
[13] G. Andersson, K. Aits, B. Hjörvarsson, J. Alloys Compd. 334 (2002) 14.
[14] H. Yukawa, D. Yamashita, S. Ito, M. Morinaga, S. Yamaguchi, J. Alloys Compd. 356–357 (2003) 45.
[15] T. Mütschele, R. Kirchheim, Scripta Met. 21 (1987) 1101.
[16] M. Dornheim, Ph.D. thesis, Universität Göttingen, 2002.
[17] D.I. Bolef, J. Appl. Phys. 32 (1961) 100.
[18] G. Alefeld, J. Völkl, Hydrogen in Metals I, Topics in Applied Physics, vol. 28, Springer-Verlag, Berlin, 1978 (Chapter 3).
[19] Y. Fukai, The Metal–Hydrogen System, 2nd ed., Springer-Verlag, Berlin, 2005.
[20] W. Lohstroh, R.J. Westerwaal, J.L.M. van Mechelen, C. Chacon, E. Johansson, B. Dam, R. Griessen, Phys. Rev. B 70 (2004) 165411.
[21] A. Pundt, M. Getzlaff, M. Bode, R. Wiesendanger, R. Kirchheim, Phys. Rev. B 61 (2000) 9964.
[22] A. Pundt, K. Nörthemann, S. Schmidt, J. Alloys Compd., accepted for publication.